Hierarchical ZnO/Bi2O3 nanostructures : synthesis, characterization, and electron-beam modification

Ling, Bo; Sun, Xiaowei; Shen, Yiqiang; Dong, Zhili

2010

Ling, B., Sun, X., Shen, Y., & Dong, Z. (2010). Hierarchical ZnO/Bi2O3 nanostructures: synthesis, characterization, and electron-beam modification. Applied physics A, 98(1), 91-96.

https://hdl.handle.net/10356/79887

https://doi.org/10.1007/s00339-009-5431-8

Hierarchical ZnO/Bi_2O_3 nanostructures: synthesis, characterization, and electron-beam modification

Bo Ling · Xiao Wei Sun · Yi Qiang Shen · Zhi Li Dong

B. Ling • X.W. Sun (✉)
School of Electrical and Electronic Engineering, Nanyang Technological University, Singapore 639798, Singapore
e-mail: exwsun@ntu.edu.sg Fax: +65-6792-0415
Y.Q. Shen • Z.L. Dong (✉)
School of Materials Science and Engineering, Nanyang Technological University, Singapore 639798, Singapore
e-mail: zldong@ntu.edu.sg Fax: +65-6790-9081

Abstract Two types of ZnO/Bi_2O_3 nanonecklace heterostructures were fabricated using the vapor-phase transport (VPT) method for the first time. These hierarchical structures were well characterized by X-ray diffraction (XRD), field-emission scanning electron microscopy (FESEM), and transmission electron microscopy (TEM) with energy dispersive spectroscopy (EDS) attached. The growth mechanism of the novel structures were proposed based on these characterizations. Electron-beam irradiation was found to be a powerful and controllable tool in further tailoring such ZnO/ Bi_2O_3 nanonecklace heterostructures. In addition, photoluminescence (PL) emission from the hierarchical nanostructures showed enhancement comparing to the pure Bi_2O_3 powder.

PACS 61.46.-w · 61.82.Fk · 81.07.-b · 81.16.Be

1 Introduction

One-dimensional (1D) nanostructures have attracted tremendous interest due to their unique optical, electrical, and chemical properties and widespread applications in nanoelectronic devices [1–4]. Moreover, novel and modulated properties can be expected from combined nanosystems consisting of two different semiconductor materials, which should expand the scope of functional heterojunctions for potential applications. Among the various methods of assembling nanomaterials, “bottom up” growth has been considered as the most effective and feasible way for fabricating nanodevices [5, 6]. Many approaches, such as vapor-phase transport (VPT) [2, 7, 8], metalorganic chemical vapor deposition (MOCVD) [9], and chemical beam epitaxy [10], have been reported to fabricate the 1D heterostructures. ZnO-based 1D heterostructures are of peculiar interest among the semiconducting oxides due to its superior optical and electronic properties and potential application in nanoscale transistors, sensors, and ultraviolet (UV) laser diodes [7, 11]. Although considerable efforts have been devoted to the synthesis and

characterization of ZnO-based bulk heterostructures, reports on the formation of 1D Zn-Obased heterostructures are rare. This is especially true for the case of ZnO/ Bi_2O_3 nanosystem [12] which could be potentially applied as photocatalysts, nanovaristors, nano light-emitting diodes (LEDs), nanosensors, and transistors.

In this paper we shall report the first synthesis of two types of ZnO/Bi_2O_3 nanonecklace heterostructures, namely, Bi_2O_3 -decorated ZnO nanorod heterostructure and Bi_2O_3 -decorated Bi_2O_3 /ZnO core–shell heterostructure. Until now there are few reports on the synthesis of nanonecklace structure composed of other semiconductor materials based on nanorod string [8, 13] and no literature reported on the synthesis of nanonecklace structure based on core–shell string, to the best of our knowledge. Interestingly, we also find that electron-beam irradiation is an effective tool for further tailoring the nanonecklace system. Bi_2O_3 beads and cores can be selectively removed and the length of ZnO nanorods can also be adjusted by cutting. Those novel nanoheterostructure systems may not only be useful for fundamental physical research but also provide a new nanosystem for further application in various nanodevices.

2 Experimental details

Self-organized ZnO/ Bi_2O_3 nanonecklace heterostructures were synthesized by the VPT method from ZnO (99.99%, AlfaAesar), Bi_2O_3 (99.999%, Strem Chemicals), and graphite powder in a mass ratio of 2:2:1 on Si (100) substrates without the presence of any catalyst. In brief, a small quartz tube containing the source and the Si substrate was inserted into a horizontal quartz tube furnace at 950°C. The furnace was kept at about 1 Torr with a rotary pump with a constant flow of 130 sccm Ar and 1.5 sccm O_2 for 30 min, after which the small quartz tube was pulled out and cooled down to the room temperature. A layer of light-yellow product was deposited on the substrate.

The crystal structure and morphology of the as-prepared products were characterized by 2θ-scan X-ray diffraction (XRD, Rigaku, operated at 40 kV, 40 mA), field-emission scanning electron microscopy (FESEM, JSM-6340F, operated at 5 kV), transmission electron microscopy (TEM, JEM-2010, operated at 200 kV). For TEM irradiation study, current density is approximately 163.2 pA/cm2 and the magnification is 8000×. For TEM characterization, the obtained heterostructures were ultrasonically dispersed in ethanol and dripped onto the carbon coated cooper grid. The chemical composition and element mapping analysis were carried out using energy dispersive spectroscopy (EDS) attached to TEM. Room-temperature photoluminescence (PL) measurements were performed using a He–Cd 325-nm laser as the excitation source.

3 Results and discussion

Figure 1a shows the scanning electron microscopy (SEM) images of ZnO/Bi_2O_3 nanonecklace heterostructure synthesized by VPT method. The high-magnification SEM image of the heterostructure (inset of Fig. 1a) gives a clear view of the unique nanonecklace structure. The hierarchical structures consist of nanorods as strings and small particles wrapped outside in sequence as beads. The diameters of the nanorods and beads are ranging from 30 to 250 nm and from 50 to 500 nm, respectively. The length of such self-organized ZnO/ Bi_2O_3 nanonecklace heterostructure can be up to tens and even hundreds micrometers. Figure 1b shows the X-ray diffraction (XRD) pattern of the ZnO/ Bi_2O_3 nanonecklace heterostructure indicating clearly that the nanoheterostructures are mainly composed of two crystalline phases, i.e., tetragonal β- Bi_2O_3 (ICSD #62979: a = 7.741 Å and c = 5.634 Å) and hexagonal wurtzite ZnO (ICSD #67454: a = 3.2501 Å and c = 5.2071 Å). Other than these two main crystalline phases, three small peaks were also detected and can be indexed to rhombohedral Bi (ICSD #64705: a = 4.533 Å, c = 11.797 Å). The detection of metallic Bi suggests that there is some metallic Bi remained in the structures which could be probably in the core of the heterostructures. Transmission electron microscopy (TEM) images shown in Figs. 1c and 1d revealed two types of interesting heterostructures which cannot be distinguished by SEM. The nanonecklace heterostructures were found to have two typical morphologies throughout the sample, i.e., nanorod heterostructure with beads (Fig. 1c) and core–shell nanorod heterostructure with beads (Fig. 1d). It is worth mentioning that the beads decorated core–shell nanorod heterostructure is dominant in the sample (~85% of the whole sample).

To investigate the crystal structure and element distribution, high-resolution transmission electron microscopy (HRTEM), selected-area electron diffraction (SAED), and EDS were carried out to probe the two types of nanorod heterostructures. A typical low-magnification TEM image of a bead-decorated core–shell nanorod heterostructure is shown in Fig. 2a. The inset of Fig. 2a shows the SAED pattern of the shell (the rectangular region marked in Fig. 2a), which is along the $[10\bar{1}0]$ zone axis of ZnO. The corresponding HRTEM image of the shell (Fig. 2b) shows well-resolved lattice fringes, revealing the single-crystalline nature of the shell. The lattice fringes have a clear sixfold symmetry and a separation of 0.26 and 0.28 nm corresponding to the d-spacing between {0002} planes and $\{10\bar{1}0\}$ planes in the ZnO wurtzite structure, respectively. The fast Fourier transform (FFT) pattern (inset of Fig. 2b) derived from the HRTEM image has been verified to show a perfect match with the SAED pattern obtained from the same region in Fig. 2a. From the HRTEM image, in conjunction with the analysis of electron diffraction and FFT patterns, the nanonecklace heterostructure is revealed to grow along the [0001] axis of wurtzite ZnO. The thickness of the ZnO shell in the Bi_2O_3 decorated ZnO/ Bi_2O_3 nanonecklace heterostructure is ~35 nm and the diameter of core is estimated to be ~120 nm. The electron microscopy investigations of the nanorod in another nanonecklace heterostructure (Fig. 1c) show the same structure as the shell in Fig. 1d confirming the nanorod to be single-crystalline ZnO.

To further verify the compositions of the decorated particles and core in these two nanonecklace heterostructures, EDS analysis has been carried out in both nanostructures. The EDS spectra shown in Figs. 2c and 2d have been acquired from region A (Fig. 1c) and B (Fig. 1d), respectively. Considering the Cu peak originates from the copper grid holder, it was found that only Zn, Bi, and O elements were detected in the EDS spectra, which correlates well with the XRD measurement. The same elements were detected from these two nanonecklace heterostructures with only slightly higher Bi content in region B (Bi:Zn = 23:21) than that in region A (Bi:Zn = 22:22). This could be attributed to the existing of Bi_2O_3 core in the ZnO shell in region B. Furthermore, EDS elemental mapping was also carried out to investigate the distribution of the two crystalline materials in the nanonecklace heterostructures. The elemental mapping of Zn, Bi, and O from these two nanonecklace heterostructures are shown in Figs. 2e and 2f, respectively. It was found that oxygen is uniformly distributed in both nanoheterostructures, and Bi mainly exists in the core and particle regions, while Zn is in nanorod and shell structures. As a result, the two nanonecklace heterostructures were confirmed to be Bi_2O_3 beads decorated ZnO nanorods and Bi_2O_3 beads decorated Bi_2O_3 /ZnO core–shell nanorods.

The formation of the self-organized ZnO/ Bi_2O_3 nano-necklace heterostructures can be explained by self-catalyzed vapor–liquid–solid (VLS) mechanism for initial nucleation and traditional vapor–solid (VS) mechanism for subsequent growth [14, 15]. Figure 3a shows the schematic illustration of the overall growth evolution of two kinds of ZnO/ Bi_2O_3 heterostructures. At high temperature region, Bi_2O_3 and ZnO powder were reduced by graphite into Bi and Zn vapors. Carried by Ar gas, the Bi and Zn vapors were transported to the low temperature region forming droplets of a Bi, Zn, and Bi/Zn mixture. We attribute the different nanostructures formed in our experiments to the different composition of the initial droplets. Since the boiling point of Zn (907°C) is much lower than that of Bi (1564°C), the Zn vapor would dominate at the beginning of the reaction. In addition, the melting point of Zn (419.53°C) is higher than that of Bi (271.5°C). Therefore, using Zn is relatively easier to form droplet on the Si substrate. Bi vapor carried by Ar gas may be absorbed in these initial Zn droplets or arrived together with Zn vapor to form Zn–Bi alloy droplets in the low temperature region, which were quickly oxidized to form nuclei in the oxidation atmosphere. Because the melting point of ZnO (1975°C) is higher than that of Bi_2O_3 (824°C), Zn combine with O2 around and form nuclei much more quickly [16]. For initial Zn droplets, they developed into ZnO nanorod; for initial Zn–Bi alloy droplets, they developed into Bi_2O_3 / ZnO core–shell structures. Also, in some cases when Zn was quickly oxidized or the Bi content is very low in the alloy droplet, Bi droplet might be totally confined in ZnO shell thus preventing them from being further oxidized. This may be the reason why Bi peak can also be detected in our previous XRD spectrum (Fig. 1b). During the development of these ZnO nanorods and Bi_2O_3/ ZnO core–shell structures, further adsorption of Zn and Bi vapor results in continuing growth of ZnO along [0001] direction and decorated particles wrapped outside.

PL measurements of the synthesized ZnO/ Bi_2O_3 heterostructures were performed at room temperature using a He–Cd laser line of 325 nm as the excitation source. For comparison, the PL of the commercial ZnO and Bi_2O_3 powders were also examined. As shown in Fig. 3b, the ZnO/ Bi_2O_3 heterostructures exhibit a broad green emission peaking at ~530 nm. Although both PL spectra of ZnO and Bi_2O_3 show dominant green emission peaks, the normalized PL spectra from ZnO shows a good overlap with that of the ZnO/Bi_2O_3 heterostructure (inset in Fig. 3b). This indicates that the green emission from the ZnO/Bi_2O_3 heterostructure is primarily coming from ZnO [17, 18]. Moreover, by comparing the PL spectra of Bi_2O_3 and ZnO/Bi_2O_3 system in the long wavelength range (>700 nm), we can see that the emission from Bi_2O_3 is clearly present in the ZnO/Bi_2O_3 heterostructure (Fig. 3b). Thus, the PL from ZnO/Bi_2O_3 heterostructure comes from both ZnO and Bi_2O_3 with the ZnO emission dominating.

It is worth mentioning here that the nanonecklace heterostructures can be further tailored by electron-beam irradiation. During TEM observations, we found that Bi_2O_3 beads and cores may be easily melted under electron-beam irradiation, as a result of the lower melting point of Bi_2O_3 com-pared to that of ZnO. Figures 4a–i show the structure development depend on the exposure time (0–110 s). A Bi_2O_3 - bead-decorated Bi_2O_3 /ZnO core–shell nanonecklace structure is displayed in Fig. 4a. It can be seen that during the first 8 s under electron-beam irradiation, the Bi_2O_3 beads melted and were solidified onto the edge of a nearby carbon film (denoted by the rectangular region in Fig. 4c). In addition to Bi_2O_3 beads tailoring, we utilized stronger electron-beam irradiation to cut the ZnO shell by converging the electron beam to a small area (denoted by the circle in Fig. 4c). After another 7 s, the ZnO shell ruptured due to sudden expansion of Bi_2O_3 core when melting (Fig. 4d). Further irradiation of the Bi_2O_3 /ZnO core–shell nanorod, the melted Bi_2O_3 core will gradually move out of the ZnO shell from the raptur(denoted by the arrows in Fig. 4e) thus finally forming the ZnO nanotube (Fig. 4i). Insets in Figs. 4h and 4i show the tip of the ZnO nanotube, which indicate the Bi_2O_3 core can also move out from the opening end of the ZnO nanotube. According to the Figs. 4a–i, it was found that Bi_2O_3 decorated Bi_2O_3 /ZnO core–shell structures can be easily tailored into Bi_2O_3 /ZnO core–shell nanorod and ZnO nanotube depending on the different exposure time. Also the Bi_2O_3 beads and core can be selectively removed by converging the electron beam in a specific region.

4 Conclusions

In conclusion, we report a single-step approach to synthesize the novel heterostructures of ZnO/Bi_2O_3 nanonecklace for the first time without the presence of any catalyst or template. The growth mechanism was proposed to be self-catalyzed VLS process combined with VS process based on systematic structure characterizations. Initial droplets for nucleation play an important role in determining the formation of two different nanostructures. PL measurement showed that the ZnO/Bi_2O_3 nanonecklace heterostructures had an intense visible light emission at ~530 nm.

Electron-beam irradiation was found to be a powerful tool for further tailoring such ZnO/Bi_2O_3 nanonecklace heterostructures.The synthesis and structure tailoring of ZnO/ Bi_2O_3 nano-necklace heterostructures offer new composite nanosystems for both fundamental research in nanoscale and fabrication of advanced nanoscale electronic and photoelectronic devices.

References

1. J.T. Hu, M. Ouyang, P.D. Yang, C.M. Lieber, Nature **399**, 48 (1999)

2. M.S. Gudiksen, L.J. Lauhon, J. Wang, D.C. Smith, C.M. Lieber, Nature **415**, 617 (2002)

3. Y.Y. Wu, R. Fan, P.D. Yang, Nano Lett. **2**, 83 (2002)

4. J. Luo, L. Zhang, Y.J. Zhang, J. Zhu, Adv. Mater. **14**, 1413 (2002)

5. M.T. Björk, B.J. Ohlsson, C. Thelander, A.I. Persson, K. Deppert, L.R. Wallenberg, L. Samuelson, Appl. Phys. Lett. **81**, 4458 (2002)

6. L. Samuelson, Mater. Today **6**, 22 (2003)

7. L.W. Yin, M.S. Li, Y. Bando, D. Golberg, X.L. Yuan, T. Sekiguchi, Adv. Funct. Mater. **17**, 270 (2007)

8. J.F. Tian, X.J. Wang, L.H. Bao, C. Hui, F. Liu, T.Z. Yang, C.M. Shen, H.J. Gao, Cryst. Growth Des. **8**, 3160 (2008)

9. F. Qian, Y. Li, S. Gradecak, D. Wang, C.J. Barrelet, C.M. Lieber, Nano Lett. **4**, 1975 (2004)

10. L. Samuelson, C. Thelander, M.T. Björk, M. Borgströma, K. Depperta, K.A. Dicka, A.E. Hansena, T. Mårtenssona, N. Paneva, A.I. Perssona, W. Seiferta, N. Sköldа, M.W. Larssonb, L.R. Wallenbergb, Physica E **25**, 313 (2004)

11. J.W. Liu, X.J. Li, L.M. Dai, Adv. Mater. **18**, 1740 (2006)

12. C.K. Xu, K. Rho, J. Chun, D.E. Kim, Nanotechnology **17**, 60 (2006)

13. H. Ni, X.D. Li, Appl. Phys. Lett. **89**, 053108 (2006)

14. S. Kar, B.N. Pal, S. Chaudhuri, D. Chakravorty, J. Phys. Chem. B **110**, 4605 (2006)

15. L. Kumari, J.H. Lin, Y.R. Ma, J. Phys. Condens. Matter **19**, 406204 (2007)

16. Y.B. Li, Y. Bando, D. Golberg, Adv. Mater. **15**, 581 (2003)

17. B.D. Yao, Y.F. Chan, N. Wang, Appl. Phys. Lett. **81**, 757 (2002)

18. Y. Yang, J.X. Wang, X.W. Sun, B.K. Tay, Z.X. Shen, Y.Z. Zhou, Nanotechnology **18**, 055709 (2007)

List of figures

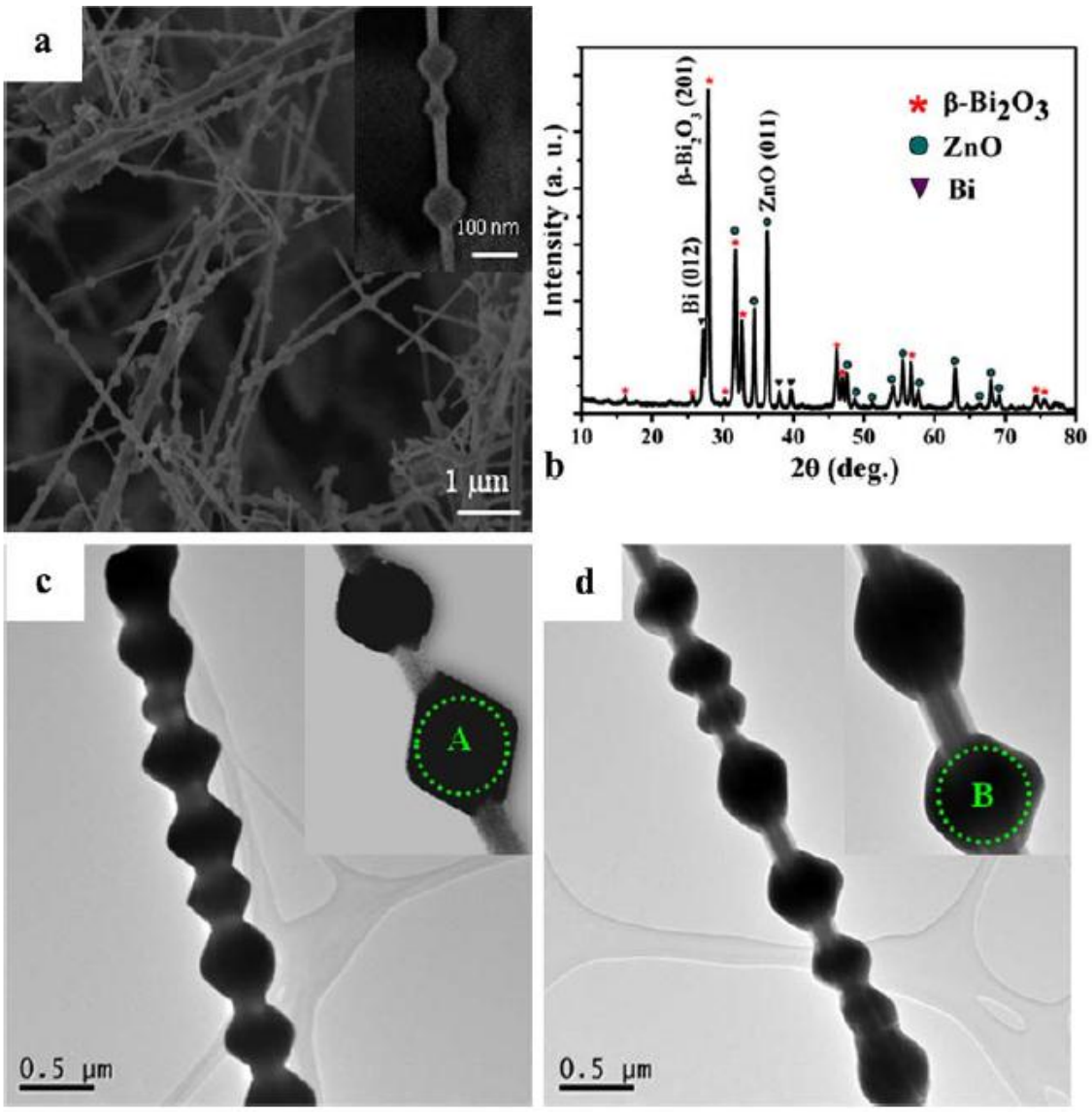
a
100 nm
1 μm
b
Intensity (a. u.)
β-Bi2O3 (201)
Bi (012)
ZnO (011)
β-Bi2O3
ZnO
Bi
10
20
30
40
50
60
70
80
2θ (deg.)
c
A
0.5 μm
d
B
0.5 μm

Fig.1

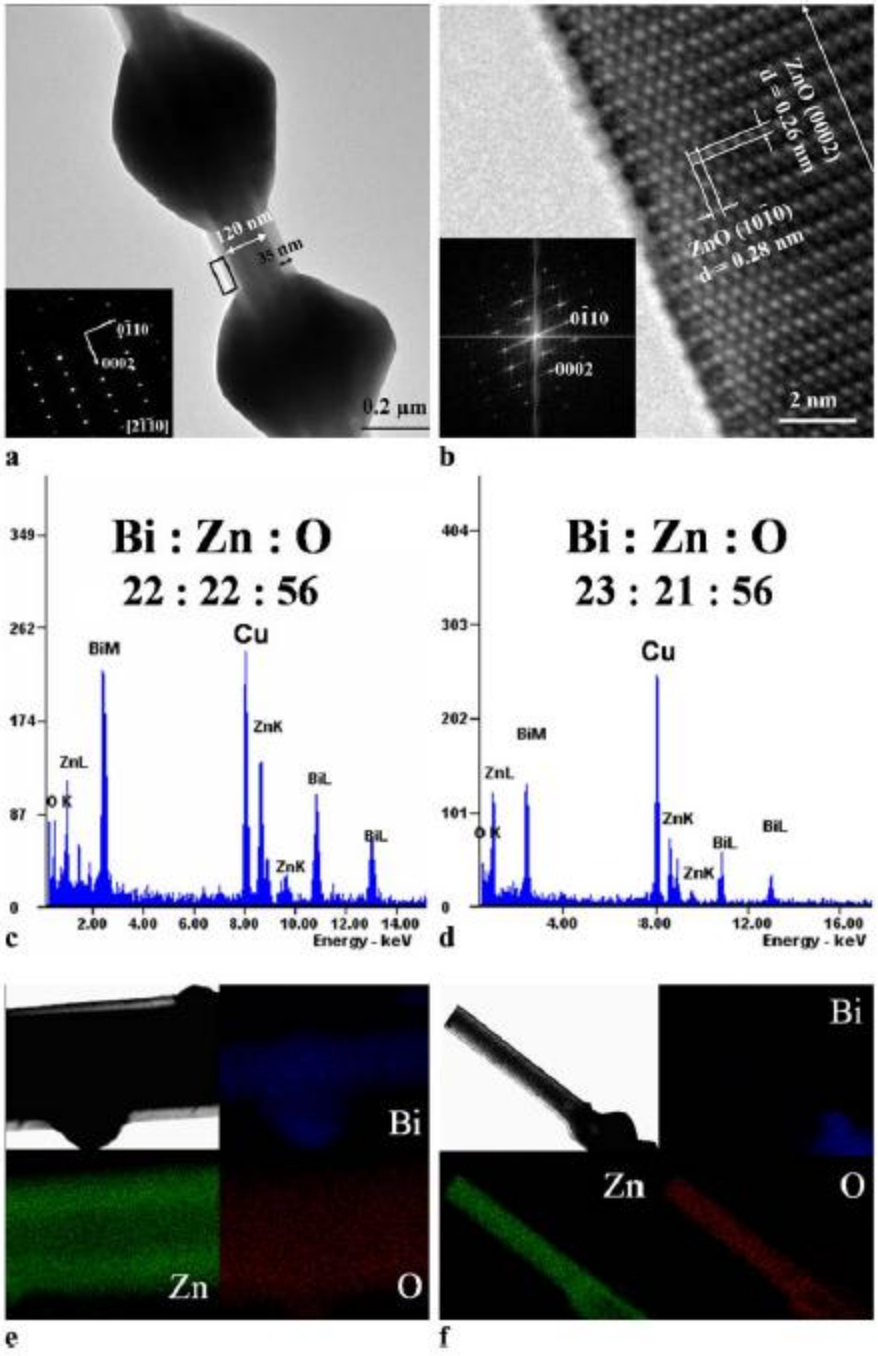
120 nm
35 nm
0.2 μm
[2$\bar{1}$$\bar{1}$0]
0$\bar{1}$10
0002
a
ZnO (0002)
d = 0.26 nm
ZnO (10$\bar{1}$0)
d = 0.28 nm
-0$\bar{1}$10
-0002
2 nm
b
Bi : Zn : O
22 : 22 : 56
BiM
Cu
ZnK
ZnL
O K
BiL
ZnK
BiL
Energy - keV
c
Bi : Zn : O
23 : 21 : 56
Cu
BiM
ZnL
O K
ZnK
BiL
ZnK
BiL
Energy - keV
d
Bi
Zn
O
e
Bi
Zn
O
f

Fig.2

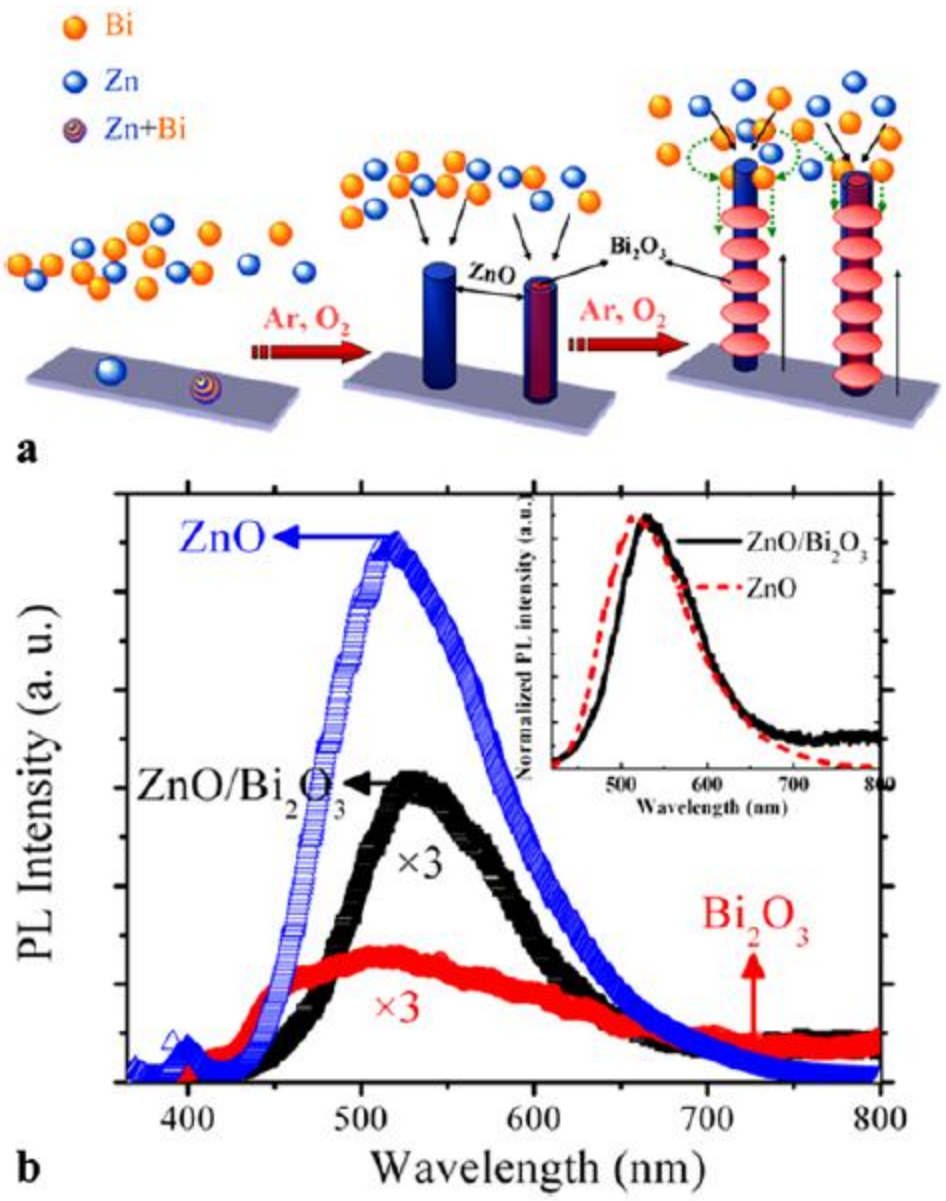
Bi
Zn
Zn+Bi
ZnO
Bi_2O_3
Ar, O_2
Ar, O_2
a
ZnO
ZnO/Bi_2O_3
×3
×3
Bi_2O_3
PL Intensity (a. u.)
400
500
600
700
800
Wavelength (nm)
b
Normalized PL intensity (a.u.)
ZnO/Bi_2O_3
ZnO
500
600
700
800
Wavelength (nm)

Fig.3

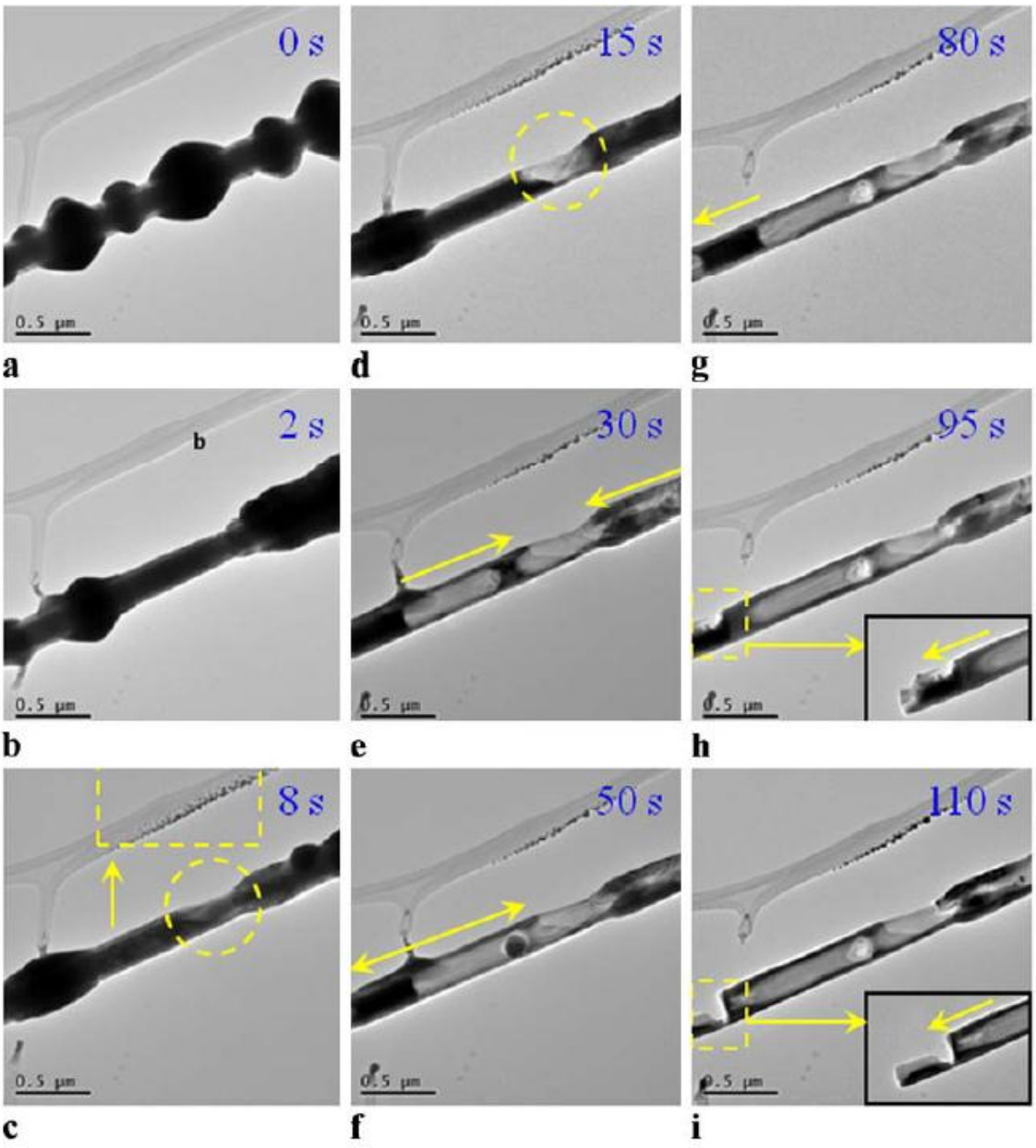

Fig.4